

Quantum teleportation of a genuine vacuum–one-photon qubit generated via a quantum dot source

Beatrice Polacchi,¹ Francesco Hoch,¹ Giovanni Rodari,¹ Stefano Savo,¹
Gonzalo Carvacho,¹ Nicolò Spagnolo,¹ Taira Giordani,^{1,*} and Fabio Sciarrino¹

¹*Dipartimento di Fisica - Sapienza Università di Roma, P.le Aldo Moro 5, I-00185 Roma, Italy*

Quantum state teleportation represents a pillar of quantum information and a milestone on the roadmap towards quantum networks with a large number of nodes. Successful photonic demonstrations of this protocol have been carried out employing different qubit encodings. However, demonstrations in the Fock basis encoding are challenging, due to the impossibility of creating a coherent superposition of vacuum-one photon states on a single mode with linear optics. Previous realizations using such an encoding strongly relied on ancillary modes of the electromagnetic field, which only allowed the teleportation of subsystems of entangled states. Here, we enable quantum teleportation of genuine vacuum-one photon states avoiding ancillary modes, by exploiting coherent control of a resonantly excited semiconductor quantum dot in a micro-cavity. Within our setup, we can teleport vacuum-one-photon qubits and perform entanglement swapping in such an encoding. Our results may disclose new potentialities of quantum dot single-photon sources for quantum information applications.

INTRODUCTION

Quantum teleportation [1–3] is one of the most intriguing processes arising from the theory of quantum mechanics, being at the core of quantum technologies as well as to the development of many concepts in quantum information theory. This protocol is enabled by a shared quantum entangled resource. A quantum state is jointly measured with one-half of the entangled resource in a given place and, as a result of such an operation, it is transferred to the other half in a remote location. Such a protocol, together with entanglement swapping [4, 5], is at the core of several quantum computation [6, 7] and quantum communication schemes ranging from quantum repeaters [8, 9], quantum gate teleportation [10–12], measurement-based quantum computing [13–15] as well as port-based quantum teleportation [16, 17]. Over the years, several experiments have successfully shown the teleportation of unknown quantum states using different experimental setups and degrees of freedom [2, 3, 18–26]. In particular, the first platforms were based on photonic systems [2, 3], since photons represent natural information carriers, due to their low interaction with the environment and to the capability of their efficient manipulation through linear optics. Quantum teleportation has been implemented over hundreds of kilometers using free-space channels [27, 28], across metropolitan networks [29–31], using satellites stations [32] and near-deterministic single-photon sources [33]. All protocols implemented with a photon-based platform have to take into account the impossibility of performing a complete deterministic Bell measurement with linear optics. Indeed, this is only feasible in a non-deterministic way, by exploiting suitably prepared ancillary qubits and

post-selection procedures [6, 7, 34] or, alternatively, by exploiting nonlinear optics, with very low success rates [24]. In this context, a major challenge consists in teleporting qubits encoded in the photon-number basis, since generating photon-number superposition states on a single electromagnetic mode is unfeasible only by means of linear optical elements. This specific example of a quantum teleportation encoding was firstly considered in [21] and then in [25]. The scheme considered the teleportation of a vacuum-one-photon qubit, produced by making a photon impinging on a beam splitter and encoding the qubit into one of the two output modes. Hence, the production of photon-number states is performed by using an ancillary mode of the electromagnetic field to encode the state to be teleported. Consequently, as also stated by the authors, the teleported state is, in fact, not a *genuine* vacuum-one-photon qubit, but a subsystem of an entangled state, making this scheme more similar to entanglement swapping.

Here, we propose a way to overcome such limitations, based on the nonlinear features enabled by the resonant excitation of a quantum dot single-photon source [35, 36]. Recent advances in the quantum dot sources technology have enabled a significant step forward in the generation of photonic states for quantum information protocols [37–43]. Our approach relies on the generation of single photons through resonant optical excitation of a quantum dot in a microcavity [38, 44], which was recently shown to be able to produce coherent superposition states of vacuum and one photon [45], as well as photon-number entangled states [46]. This is due to its capability of transferring the coherence of the excited-ground atomic state to the generated photons [38, 45]. By harnessing this property, we were able to precisely control the vacuum-one-photon state to be teleported, as shown by the achieved results. Moreover, we also perform the entanglement swapping scheme in the spirit of

* Corresponding author: taira.giordani@uniroma1.it

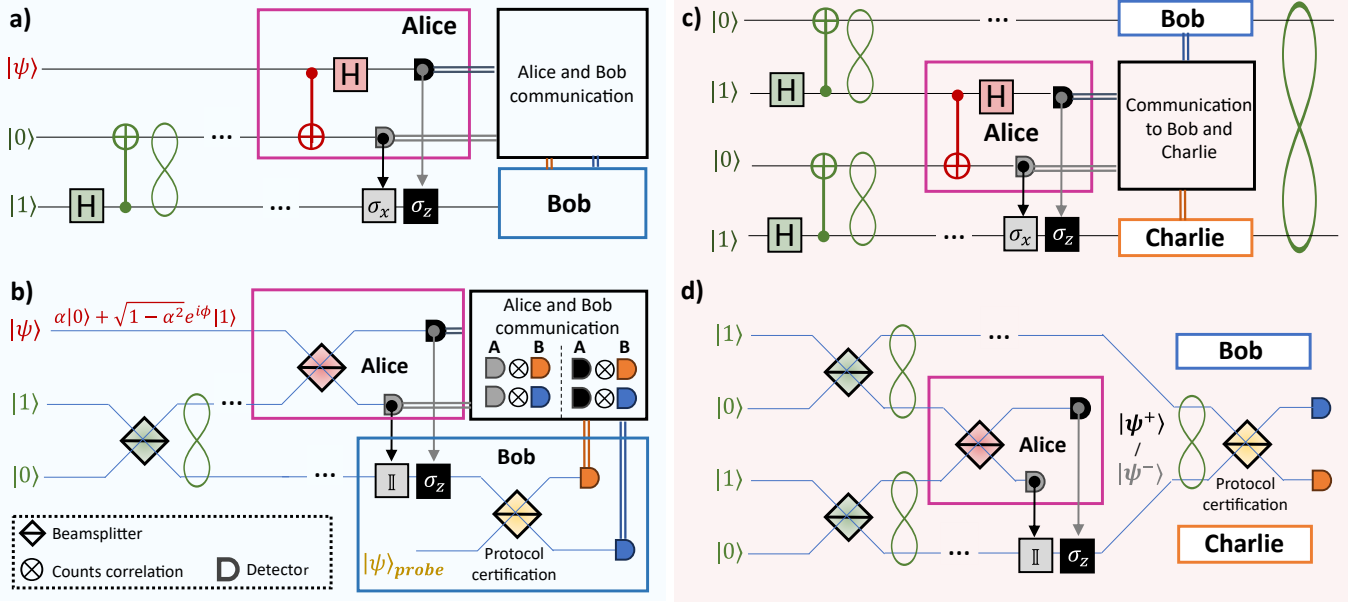


Figure 1. **Teleportation of vacuum-one-photon qubits and entangled swapping.** a) Standard circuits for quantum teleportation. The Bell state generated by the Hadamard (H) and CNOT gates (in green) is shared between Alice and Bob. Alice performs a Bell measurement (in red) between the qubit $|\psi\rangle$ to teleport and one of the two qubits in the Bell state. Bob retrieves the qubit $|\psi\rangle$ by applying σ_x and/or σ_z according to Alice’s measurement outcomes. b) Circuit realization of a probabilistic quantum teleportation protocol in the vacuum-one-photon qubits encoding. The Bell state generation (green) and a probabilistic Bell measurement (red) are realized through the interference of single photons in a beamsplitter (BS). Alice communicates the outcomes of the measurement to Bob. Bob applies accordingly the identity or σ_z and certifies the teleportation by a self-homodyne detection with a reference state performed by the last yellow BS. c) Circuitual scheme of the entanglement swapping protocol. Alice performs a Bell measurement on two qubits that belong to two independent Bell states. Bob and Charlie will share a Bell state after the communication of Alice’s measurement outcomes and the consequent applications of σ_x or/and σ_z operators on Charlie’s qubit. d) Entanglement swapping in the vacuum-one-photon encoding. Two single photons enter in two different BSs (in green) that generate two Bell states. Alice performs the probabilistic Bell measurement (red BS) and communicates to Charlie and Bob which detector clicks. Then, Charlie applies the identity or σ_z . Bob and Charlie perform a further probabilistic Bell measurement to identify the entangled state they share.

the previous demonstrations of teleportation using the vacuum-one-photon paradigm [21, 25]. The results are highly compatible with the expectations, demonstrating that our platform allows for teleportation of both entangled and single qubit states in the Fock basis encoding.

Our experiment represents a step forward in the field of quantum communication, being the first example of genuine quantum teleportation of a pure state in the Fock basis, and stimulating further investigations in protocols involving photon-number encoded states [46] for quantum information tasks. Furthermore, our results may offer exciting prospects for the development of quantum dot-based advanced quantum technologies.

RESULTS

We now discuss the details of our experiment. This section is divided into three parts: in the first part, we describe the conceptual scheme of our quantum teleportation and entanglement swapping protocols using the vacuum-one photon encoding, in the second part we il-

lustrate our experimental setup while, in the third part, we report and discuss our experimental results.

A. Quantum teleportation and entanglement swapping in the vacuum-one-photon encoding

Here, we first briefly review the quantum teleportation and entanglement swapping protocols through their circuit representation. Then, we discuss the conceptual scheme of our teleportation and entanglement swapping protocols in the vacuum-one photon encoding.

Teleportation. In the quantum teleportation protocol, Alice aims at sending a generic state of the form:

$$|\psi\rangle = \alpha|0\rangle_L + \beta|1\rangle_L, \quad (1)$$

to Bob, in absence of a direct quantum channel, by only exploiting a classical channel and a shared Bell state. Here, the index L is used to indicate the logical qubit. From a logical point of view, reported in Fig. 1a, the Bell state is produced by applying the following transforma-

tion to an initial two-qubit state:

$$|\psi^+\rangle = \text{CNOT}(\text{H} \otimes \text{I}) |01\rangle_L. \quad (2)$$

To teleport her state, Alice performs a Bell-state measurement (BSM) between the two qubits on her stage, i.e. $|\psi\rangle$ and one half of the Bell state, obtaining a two-bit outcome. Depending on the result of such an operation, the second half of the Bell state, sent to Bob's stage, is left in one of the possible states: $\alpha |0\rangle_L + \beta |1\rangle_L$, $\alpha |1\rangle_L + \beta |0\rangle_L$, $\alpha |0\rangle_L - \beta |1\rangle_L$, or $\alpha |1\rangle_L - \beta |0\rangle_L$. Therefore, to retrieve the original state $|\psi\rangle$, Bob may need to apply a unitary transformation to his state according to Alice's two-bit outcome.

In Fig. 1b, we show the conceptual scheme of our experiment, that implements the teleportation protocol of a vacuum-one photon state, i.e. where the logical state $|0\rangle_L$ ($|1\rangle_L$) is encoded in the absence (presence) of one photon on a given electromagnetic mode. In detail, we initially generate a genuine vacuum-one photon state in the form of Eq. (1), and a Fock state $|1\rangle$. The Fock state is sent to a symmetric BS with input modes labelled as 1 and 2. This optical element transforms the creation operators according to $a_1^\dagger \rightarrow (a_1^\dagger + a_2^\dagger)/\sqrt{2}$, so that the resulting state reads:

$$|1_1 0_2\rangle \rightarrow \frac{|1_1 0_2\rangle + |0_1 1_2\rangle}{\sqrt{2}}. \quad (3)$$

In this way, following the idea of [21, 47], we generate a Bell state in the vacuum-one photon encoding. A partial BSM between the qubit $|\psi\rangle$ and half of the Bell state is performed in Alice's station by means of a further symmetric BS. Meanwhile, Bob receives the other half of the Bell state which, after Alice's BSM, is left with a success probability $p_{\pm} = 1/4$ either in the state $\alpha |0\rangle + \beta |1\rangle$ or $\alpha |0\rangle - \beta |1\rangle$, depending on Alice's measurement outcome. Finally, Bob validates the protocol by performing a suitable measurement between the received qubit and a reference state $|\psi\rangle_{\text{probe}}$. This measurement aims at witnessing the coherence between the two logical states, i.e. the vacuum and the one-photon components. As $|\psi\rangle_{\text{probe}}$, we employ a copy of the original qubit $|\psi\rangle$. Such a method, known as self-homodyne detection, allows measuring coherence by observing interference fringes in the single-photon counts at the output of the BS, as a function of the relative phase between the optical paths. The presence of such interference fringes is a signature of the coherence in the input states, since it cannot be obtained by mixed states. Additionally, its observation requires preparation of indistinguishable photons to enable quantum interference. Furthermore, the visibility of such fringes depends on the vacuum population of the two qubits [45]. Such a method can be used to characterize the output of the teleportation protocol, thus verifying that it has been carried out successfully. Further descriptions of the self-homodyne detection in our protocol can be found in the Supplementary Information.

Entanglement swapping. In the entanglement swapping protocol, whose scheme is shown in Fig. 1c, entanglement is transferred from a given pair of particles to another at distant node. In detail, two independent Bell pairs are initially generated. One-half of both pairs is sent to a central observer, Alice, who performs a BSM. The remaining particles, each belonging to initially distinct pairs, are sent to two arbitrarily distant parties, Bob and Charlie. The interaction of the two subsystems in Alice's station results in the state shared by Bob and Charlie ending up in a maximally entangled state. As in the quantum teleportation protocol, Bob and Charlie may need to apply a unitary transformation according to Alice's outcome to retrieve the initial Bell state.

In Fig. 1d, we report the equivalent circuit for entanglement swapping in the vacuum-one-photon encoding. The two Bell states (Eq. 3) are generated by two single-photon states, that are injected in two separate BSs. Then, Alice performs a partial BSM through a symmetric BS, analogously to the teleportation protocol described above. Bob and Charlie then retrieve their maximal entangled states $|\psi^+\rangle$ or $|\psi^-\rangle$ after Alice communicates the measurement outcome obtained at her stage, i.e. which of the two detectors counts. The success probability of the protocol is again $p_{\pm} = 1/4$. Certification of the output state after the entanglement swapping is then obtained via a further BSM between the modes at Bob's and Charlie's stages.

B. Experimental apparatus

Our experimental setup is depicted in Fig. 2. As a single-photon source, we use a commercially available (Quandela *e-Delight*) semiconductor quantum dot (QD). Such source consists of an InGaAs matrix placed in a nanoscale electrically controlled micropillar cavity [38] kept at cryogenic temperature (around 4K) by an *Attocube-Attodry800* He-closed cycle cryostat. The QD is optically excited by a pulsed laser resonant with the cavity characteristic wavelength (928.05 nm), in the so-called RF (resonant fluorescence) scheme [38, 44]. We achieve single photon collection by means of a single-mode fiber (SMF) located inside the cryostat and detect photons with avalanche photodiodes (APDs). Photons are separated from the residual pumping laser in a cross-polarization scheme. The nominal repetition rate of the laser amounts to 79 MHz, but we double it by introducing a delay between two consecutive pulses and then recombining them, as shown in the "Pulses preparation" section of Fig. 2a. Such a preparation stage also allows us to control the polarization of either pulse independently and, consequently, their power, as the laser light passes through a polarizing beam splitter (PBS) before optically exciting the QD. In the RF excitation scheme, an excitation power lower than the π -pulse translates into the generation of coherent vacuum-one photon states of the same form of Eq. (1), where the population of the state

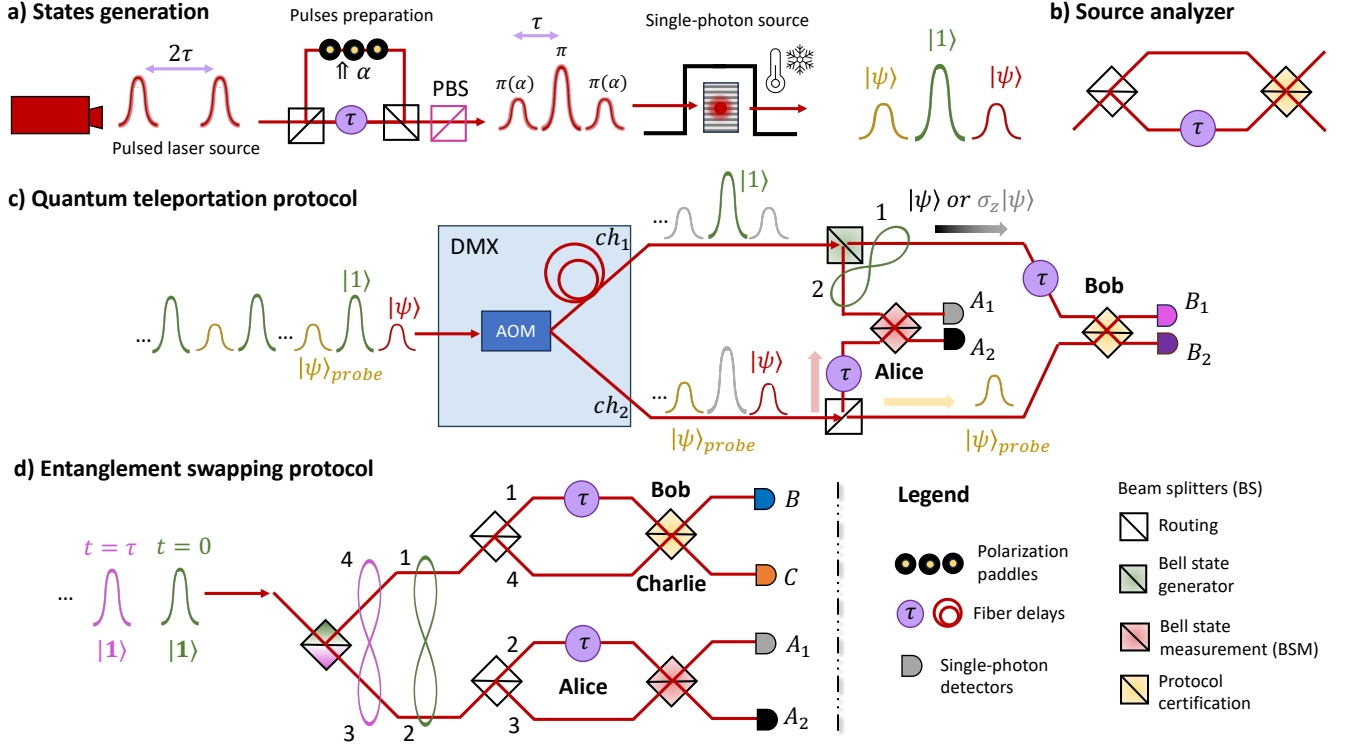


Figure 2. **Experimental setup.** a) In a first step, we doubled the repetition rate of the pump pulsed laser, from ~ 80 Mhz to ~ 160 Mhz, through an in-fiber Mach-Zehnder interferometer (MZI). Polarization paddles control the pump power of the pulses after passing through a polarizing beam-splitter (PBS). Such a modulation of the pulses power allows to resonantly excite our QD to generate sequence of states like $|\psi\rangle^{t=0}$, $|1\rangle^{t=\tau}$ and $|\psi\rangle^{t=2\tau}$, where $|\psi\rangle$ is the generic qubit of eq. 1. b) The MZI employed to characterize the vacuum-one-photon qubits generated by the source, i.e. the estimate of the α value from the visibility of the interference fringes. c) The train of states is distributed and synchronized in two different channels by a time-to-space de-multiplexer (DMX) based on an acoustic-optical modulation (AOM). In the first channel (ch_1), the $|1\rangle^{t=\tau}$ state is sent through the green BS to generate a Bell state, and, afterward, half of it interferes at time $t = \tau$ in Alice's station with $|\psi\rangle$ coming from the second channel (ch_2). The second half of the Bell state, i.e. the teleported state, is sent to Bob, who characterizes it through interference at time $t = 2\tau$ with $|\psi\rangle_{\text{probe}}$ that is a copy of the original qubit $|\psi\rangle$. The red, yellow, black arrows represent the case in which the protocol succeeds due to the probabilistic routing of $|\psi\rangle$ and $|\psi\rangle_{\text{probe}}$, as all pulses take the correct delay lines. d) We prepared a train of $|1\rangle$ states and generated Bell states at times $t = 0$ and $t = \tau$ on the first BS. Alice performs a BSM by making interfere half of the Bell state generated at $t = 0$ with half of the next entangled state generated at $t = \tau$. Bob and Charlie perform the same measurement to verify the success of the entanglement swapping protocol after the communication of Alice's station outcomes.

$|1\rangle$, i.e. $|\beta|^2$, grows with the excitation power [45], achieving the value 1 at the π -pulse. In the Methods section, we report the typical performances of the source measured with the Mach-Zehnder interferometer (MZI) of Fig. 2b for what concerns the counts rate, the second-order auto-correlation function $g^{(2)}$, the Hong-Ou-Mandel visibility and the purity of the generated vacuum-one photon qubits.

Teleportation. For the first protocol, we set the two laser pulse trains at two different powers, such to produce alternatively the states $|\psi\rangle$ and $|1\rangle$, respectively at times $t = n\tau$ and $t = (n + 1)\tau$, where $n = 0, 1, \dots$ and $\tau \approx 6$ ns. We trigger each protocol run in a way such to take as timing reference the following sequence: $|\psi\rangle_{\text{probe}}^{t=2\tau}$, $|1\rangle^{t=\tau}$, and $|\psi\rangle^{t=0}$. The generated states are sent through a Quandela commercially available temporal-to-spatial

demultiplexer (DMX) which actively separates the incoming pulses into two synchronized but spatially different ≈ 150 ns-long trains (see Fig. 2c). The $|1\rangle^{t=\tau}$ state brought by the DMX channel 1 is sent on a BS to produce the Bell state in Eq. (3). One half of such Bell state is sent to Alice, who performs a partial BSM between it and the $|\psi\rangle^{t=0}$ state brought by the DMX channel 2. The second half of the Bell state is sent to Bob, who characterizes it through interference with the $|\psi\rangle_{\text{probe}}^{t=2\tau}$ state, also brought by the DMX channel 2. More specifically, we record Bob's single counts traces conditioned on the presence of one photon in Alice's station ≈ 6 ns before, by taking a two-fold coincidence window equal to 1.5 ns. Note that the routing of $|\psi\rangle$ and $|\psi\rangle_{\text{probe}}$ is not deterministic, thus lowering the success probability to $p_{\pm} = 1/16$.

Entanglement swapping. To perform the entan-

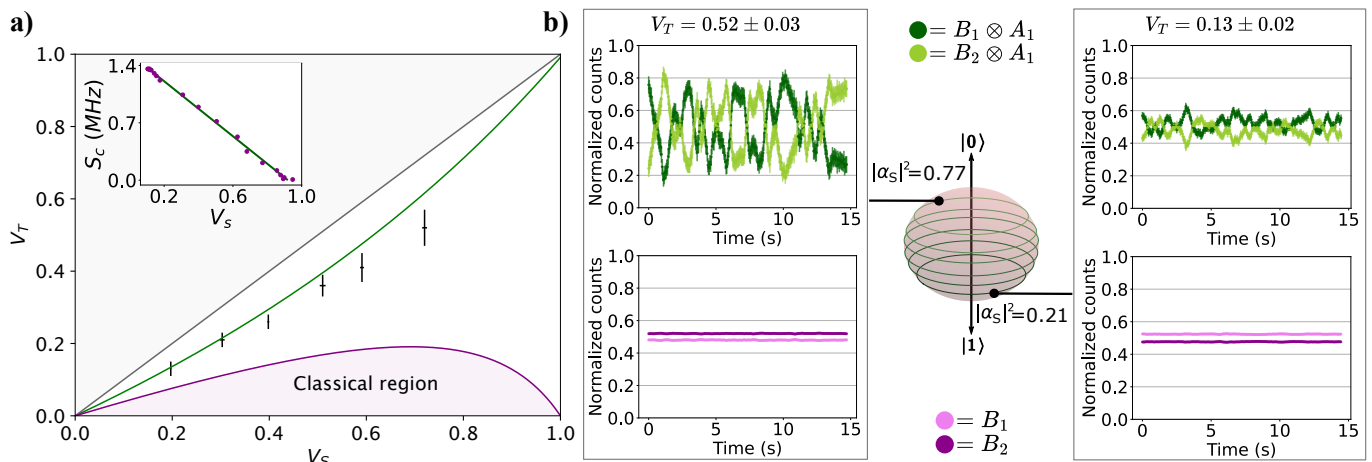


Figure 3. **Theoretical expectations and experimental results for the teleportation protocol.** **a)** In grey, we show the expected teleported visibility as a function of the probe state visibility within an ideal platform, with deterministic routing in every MZI, photon-number resolving detectors, the same self-homodyne measurement station, and perfect photon indistinguishability. The grey area is not physically accessible. In green, we show how such expectations change when considering that, in our platform, the separation of the probe and the qubit to be teleported is not deterministic and threshold detectors are employed. Furthermore, this model is formulated in the limit of high losses and considering imperfections such as state superposition purity and partial photon distinguishability. In purple, instead, we report the same quantities when using the best classical protocol in the same losses regime. In the inset, we report the single count rate (S_c) in one of two outputs of the self-homodyne station (see Fig. 2b) as a function of the visibility, for power pulse areas below or equal to π . From this plot, we estimate a state purity $\lambda \approx 0.98$. **b)** Two examples of the free evolution of the single-photon counts observed on Bob's detectors after the teleportation protocol and corresponding to two different states. The green plots show events in Bob's station, conditioned on the presence of one photon in Alice's detector number 1. In pink, instead, we show the unfiltered single count traces detected on Bob's side. Each pair of traces is normalized to the sum of the two single-photon signals. In this figure, we also illustrate that the states we are able to teleport correspond to parallel planes on the Bloch sphere, since no phase information can be retrieved with our measurements. All the shown uncertainties amount to one standard deviation and were computed by assuming Poissonian events.

glement swapping protocol, the implemented setup is shown in Fig. 2d. Unlike the teleportation protocol, we solely generate π -pulses and consider the initial state $|1\rangle^{t=\tau} |1\rangle^{t=0}$. Then, a symmetric BS generates two Bell states of the form given in Eq. (3). One half of both states is sent to Alice's Mach-Zehnder interferometer (MZI) to perform a partial BSM. The remaining half of the first Bell pair is sent to Bob, while the remainder of the second one is sent to Charlie. According to Alice's outcome, Bob and Charlie will end up with a maximally entangled state of the same form as the initial one, which they measure through interference on a BS. Suitable $t = \tau$ delays are used to synchronize the two pulses (on modes 1 and 2). Then, we measure the visibility of the state after Bob and Charlie recombined their modes in a symmetric BS. As for the teleportation protocol, we consider a two-fold coincidence window equal to 1.5 ns. The probabilistic routing of the states lowers the success probability of the protocol to $p_{\pm} = 1/16$.

C. Experimental results

Here, we report and discuss our experimental results for both the quantum teleportation and the entanglement swapping protocols.

Teleportation. To demonstrate that the teleportation protocol was successful, we analyzed the interference fringes which are obtained by the self-homodyning technique [45] described above. More specifically, the main concept is to have a quantum state, in principle unknown and that needs to be characterized, interfere on a beam splitter with a reference probe prepared in a precise state such as the qubit in Eq. (1). It can be shown (as discussed in the Methods and in the Supplementary Information) that the visibility of interference fringes leads to a direct estimation of the vacuum population of the unknown state. Furthermore, the presence of interference fringes is a genuine signature of the coherence between the vacuum $|0\rangle$ and single-photon term $|1\rangle$ in the state, given that an input mixed state results in no interference in the output pattern as a function of the phase between the modes. Characterization of the probe state is performed independently by using a time-unbalanced MZI, as the one shown in Fig. 2b. More specifically, a train of states prepared in the target state, characterized by amplitude α_S for the vacuum component, is prepared in the same spatial mode and injected in one input port of a symmetric BS. A delay τ , equal to the time separation between two input pulses, is then applied in one of the output modes of the BS. Then, the output modes interfere in a second symmetric BS, and the output fringes are measured from

the single-photon counts in each of the output modes, as a function of the relative free evolving phase in the interferometer. The visibility V_S of such a pattern provides a direct estimate of $|\alpha_S|^2$. In the inset of Fig. 3a, we show such a relationship between V_S and the single-count rate recorded by one of the two detectors at the output of the last BS, when varying the vacuum population $|\alpha_S|^2$, i.e. the power of the pump pulses. In the case of lossy apparatuses and of identical pulses such that generate trains of qubits with the same α_S , it can be shown that both the V_S and single-photon counts are linearly proportional to $|\alpha_S|^2$ (see Methods and Supplementary Information for the full derivation).

In the teleportation protocol, Bob employs a similar self-homodyne detection scheme between the unknown teleported qubit and the state $|\psi\rangle_{\text{probe}}$, that is, a copy of the original qubit. The results are shown in Fig. 3. In Fig. 3a, we compare our observations with three different theoretical models for the teleported visibility V_T of the fringes in the Bob's counts conditioned by Alice's measurements as a function of the probe state visibility V_S . In the first two models (grey and green curves) we assume correct teleportation, i.e. the teleported state is an exact copy of $|\psi\rangle$. In grey, we show the trend $V_T = V_S$ that would be observed if our setup was equipped with fully deterministic routing of $|\psi\rangle$ and $|\psi\rangle_{\text{probe}}$ (see Fig. 2c) and photon-number resolving detectors. In the green plot, instead, we show a model taking into account the features of our platform, where deterministic routing is only applied to separate the central pulse from the two copies of the $|\psi\rangle$ state, and threshold detectors are employed. The model of the green curve is formulated in the limit of high losses for both V_S and V_T , which is justified by our $\approx 10\%$ source brightness and $\approx 30\%$ detector efficiency. Furthermore, we also consider the imperfections of the source for what concerns the qubits purity and the partial photon distinguishability (see Methods and Supplementary Information for the full derivation). Finally, the purple region corresponds to what would be observed in the case of the best classical protocol as described in Ref. [48]. In this case, the classically teleported (CT) state would be the following statistical mixture: $\rho_{CT} = \frac{1}{3}|\psi\rangle\langle\psi| + \frac{1}{3}|0\rangle\langle 0| + \frac{1}{3}|1\rangle\langle 1|$ that corresponds to the state with fidelity $F = 2/3$. Our experimental observations are compatible with the green model within two standard deviations and are far from being compatible with the classical case expectations, thus showing that our protocol significantly outperforms its best classical counterpart. Instead, in Fig. 3b, we report in green (violet) our protocol performances when (not) allowing classical communication between Alice and Bob, for two different teleported coefficients $|\alpha_S|^2$. In the green plots, where Bob's single-photon counts are conditioned on the presence of one photon on one of Alice's detectors, we observe free-evolving fringes corresponding to successful teleportation. In the violet plots, instead, where Bob's single-photon counts are unfiltered, we cannot observe any fringes, due to lack of information about Alice's mea-

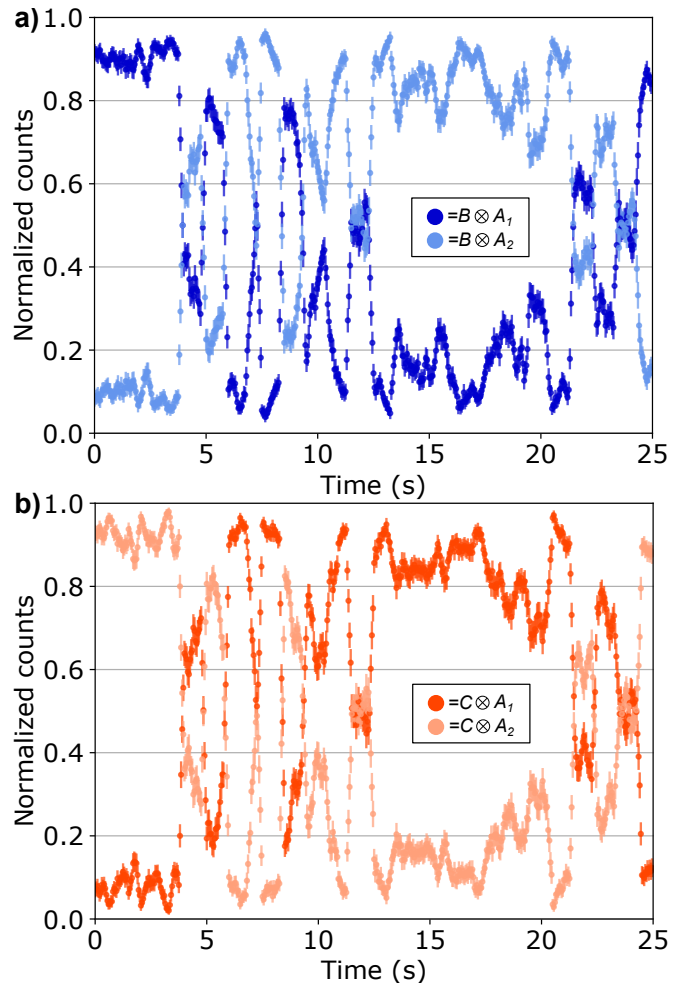


Figure 4. **Entanglement swapping in the vacuum-one-photon encoding.** a) Freely evolved fringes recorded by Bob's detector (blue and light blue data) and b) by Charlie's one (red and light red traces), triggered by the two Alice's BSM outcomes. Each pair of traces is normalized to the sum of the two single-photon signals. The uncertainties derive from the Poissonian statistics of single-photon counts.

surement outcome. The same plot illustrates that we teleport quantum states lying on a plane of the Bloch sphere, as no phase information can be retrieved with our measurements.

Entanglement swapping. As a second step, we carried out the entanglement swapping protocol according to the scheme of Fig. 2c. In Fig. 4, we show the single-count traces observed when the output modes at Bob's and Charlie's stages interfere in a BS. Indeed, similarly to the teleportation protocol, the interference fringes measured at the output can be employed as a means to verify that the entanglement swapping procedure was successful. Respectively, the measured visibilities for the four

possible two-fold events are:

$$\begin{cases} V_{A_1,C} = 0.942 \pm 0.002 \\ V_{A_1,B} = 0.862 \pm 0.002 \\ V_{A_2,C} = 0.879 \pm 0.002 \\ V_{A_2,B} = 0.903 \pm 0.002 \end{cases} \quad V_{\text{ave}} = 0.896 \pm 0.001. \quad (4)$$

As demonstrated in the Supplementary Information, in the ideal case the visibility of the state shared between Charlie and Bob at the output of the BS is 1. However, taking into account the partial distinguishability of photons, the expected visibility amounts to $V^{\text{theo}} = 0.902$ and, therefore, it is in good agreement with our experimental results. Small deviations of the individual visibilities from this ideal value are mainly due to non-ideal reflectivities of the BSs and differences in the coupling and detection efficiencies. We estimated the experimental visibility through the same method used in the previous protocol and illustrated in the Methods.

DISCUSSION

In this work, we addressed a fundamental open problem, corresponding to the quantum teleportation of a general qubit encoded in the Fock basis. Indeed, due to technological constraints, such a problem was addressed until now by using linear optics, and, in particular, BSM operations. Vacuum-one photon states were indeed generated by letting a photon impinge on a BS and taking one of the output modes as the target mode. Such a procedure results in the quantum teleportation of one subsystem of an entangled state, while not permitting the quantum teleportation of genuine qubit states in such an encoding without the use of ancillary modes. To address this issue, we exploited the nonlinear properties of a semiconductor quantum dot optically excited through resonance fluorescence. Indeed, it was recently demonstrated that such a procedure yields the production of coherent superposition states of vacuum and photon-number states. Within such a platform, we were able to quantum teleport six different pure genuine vacuum-one photon states without employing any ancillary mode, and achieving results in good agreement with expectations. Moreover, within this setup, we were able to successfully perform entanglement swapping thus further extending the potentialities of our scheme to more complex scenarios.

We believe that our findings may represent an important step toward the development of large-scale quantum networks based on photon-number basis encoding, an approach that is widely investigated in quantum computation [49, 50] and communication tasks [46, 51, 52]. Moreover, our results may encourage new applications of quantum dot-based single-photon sources for several quantum information tasks.

METHODS

Characterization of the single-photon source

We use a Hanbury-Brown-Twiss setup to measure the values of the second-order auto-correlation function $g_2(0)$ of our single-photon source and a MZI to measure the Hong-Ou-Mandel (HOM) visibility V_{HOM} , for each measurement station. For the quantum teleportation experiment, we only have two participants, Alice and Bob. For the entanglement swapping experiment, instead, we also have Charlie. However, for both experiments, we call more generally Bob's HOM visibility, the one characterizing the second MZI.

Typical values throughout the whole experiment are (see also Sec. V of the Supplementary Information):

$$\begin{aligned} g_2^{\text{Alice}}(0) &= 0.0146 \pm 0.0006, \\ g_2^{\text{Bob}}(0) &= 0.0192 \pm 0.0007, \\ V_{\text{HOM}}^{\text{Alice}} &= 0.9055 \pm 0.0015, \\ V_{\text{HOM}}^{\text{Bob}} &= 0.8987 \pm 0.0012. \end{aligned}$$

Additionally, we characterized the purity of the state generated by our single-photon source by measuring the fringe visibility for different values of the excitation power, as also suggested in [45]. Indeed, it is necessary to consider the generation of a mixed state of the form:

$$\rho_s = \lambda \rho_{\text{pure}} + (1 - \lambda) \rho_{\text{mixed}}.$$

Here $\rho_{\text{pure}} = |\psi\rangle\langle\psi|$ is a pure state, analogous to the one in Eq. (1) and encoded in the photon-number basis, while $\rho_{\text{mixed}} = \text{diag}\{|\alpha|^2, |\beta|^2\}$ is a mixture of the vacuum and one-photon populations. As demonstrated in [45], one can extract the value of λ by observing the dependence of the fringes visibility V_S from the vacuum population in a self-homodyne detection. In our apparatus, λ is retrieved from the the slope of the linear fit performed on the data in the inset of Fig. 3a. It amounts to $\lambda \approx 0.98$.

Characterization of the probe state

We characterize the probe state by using an independent procedure with respect to the protocol implementation. In detail, we observe the interference of two same probe states at the output of a standard MZI (see Fig. 2b) in Alice's station. The $|\alpha_S|^2$ coefficient is then computed from the measured fringe visibility by inverting the following formula:

$$V_S = \lambda^2 \sqrt{V_{\text{HOM}}^{\text{Alice}}} |\alpha_S|^2,$$

where λ is the state purity. We report its full formal derivation in Section I of the Supplementary Information.

Characterization of the teleported state and experimental imperfections

We characterize the teleported state by observing the fringe visibility at the output of Bob's last BS. In the hypothesis of correct teleportation, which means that the state $|\psi\rangle_{\text{probe}}$ and the teleported state have the same vacuum population $|\alpha_S|^2$, we expect that $V_T = V_S$. The imperfections of the experimental apparatus, such as the use of threshold detectors and of probabilistic routing of the states $|\psi\rangle$ and $|\psi\rangle_{\text{probe}}$, limit the value of the measured V_T , such that $V_T < V_S$. By taking into account such limitations and considering the other imperfections summarized by λ , $V_{\text{HOM}}^{\text{Alice}}$ and $V_{\text{HOM}}^{\text{Bob}}$, we derive the following formula for the visibility of the teleported state as a function of V_S :

$$V_T = \frac{2\lambda^2 \sqrt{V_{\text{HOM}}^{\text{Alice}} V_{\text{HOM}}^{\text{Bob}} V_S}}{3\lambda^2 \sqrt{V_{\text{HOM}}^{\text{Alice}} - V_S}}$$

The full derivation of such an equation is reported in Section II of the Supplementary Information. The calculation has been carried out in the regime of high losses as for the derivation of V_S .

Data analysis

We derived a procedure that improves significantly the accuracy of the measured visibility, even in the case of low event statistics, that we briefly discuss below. For details on the derivation we refer to Section III of the Supplementary. We indicate with $n(\phi(t))$ a single-photon count trace, where $\phi(t)$ is the freely evolving phase in a MZI. The visibility can be evaluated as:

$$V = \sqrt{2 \frac{\langle n^2 \rangle_t - \langle n \rangle_t^2}{\langle n \rangle_t^2}}$$

where $\langle \cdot \rangle_t$ is the time average, and for brevity we have omitted in the notation the dependence of n on $\phi(t)$. The measured single-photon count traces for the teleportation (Fig. 3b) and entanglement swapping (Fig. 4) were recorded for a time of $\sim 10^5$ bins of 50 ms that is around 1 hour. The average number $\langle n \rangle$ of photons in each time bin ranges from 5 to 100 depending on the vacuum population.

ACKNOWLEDGEMENTS

We thank *Quandela* for all the support provided. We also acknowledge support from the ERC Advanced Grant QU-BOSS (QUAntum advantage via nonlinear BOSon Sampling, grant agreement no. 884676) and from PNRR MUR project PE0000023-NQSTI (Spoke 4).

AUTHOR CONTRIBUTIONS

B.P., F.H., G.R., T.G., and F.S. conceived the experiment. B.P., G.R., F.H., S.S., T.G. carried out the experiment. F.H., B.P., G.R., S.S., G.C., N.S., T.G. and F.S. performed the data analysis. All the authors discussed the results and contributed to the writing of the paper.

COMPETING INTERESTS

The authors declare no competing interests.

DATA AVAILABILITY

The data that support the findings of this study are available from the corresponding authors upon reasonable request.

-
- [1] C. H. Bennett, G. Brassard, C. Crépeau, R. Jozsa, A. Peres, and W. K. Wootters, Teleporting an unknown quantum state via dual classical and einstein-podolsky-rosen channels, *Phys. Rev. Lett.* **70**, 1895 (1993).
 - [2] D. Bouwmeester, J.-W. Pan, K. Mattle, M. Eibl, H. Weinfurter, and A. Zeilinger, Experimental quantum teleportation, *Nature* **390**, 575 (1997).
 - [3] D. Boschi, S. Branca, F. De Martini, L. Hardy, and S. Popescu, Experimental realization of teleporting an unknown pure quantum state via dual classical and einstein-podolsky-rosen channels, *Phys. Rev. Lett.* **80**, 1121 (1998).
 - [4] M. Żukowski, A. Zeilinger, M. A. Horne, and A. K. Ekert, “event-ready-detectors” bell experiment via entanglement swapping, *Phys. Rev. Lett.* **71**, 4287 (1993).
 - [5] J.-W. Pan, D. Bouwmeester, H. Weinfurter, and A. Zeilinger, Experimental entanglement swapping: Entangling photons that never interacted, *Phys. Rev. Lett.* **80**, 3891 (1998).
 - [6] D. Gottesman and I. L. Chuang, Demonstrating the viability of universal quantum computation using teleportation and single-qubit operations, *Nature* **402**, 390 (1999).
 - [7] E. Knill, R. Laflamme, and G. J. Milburn, A scheme for efficient quantum computation with linear optics, *Nature* **409**, 46 (2001).
 - [8] H.-J. Briegel, W. Dür, J. I. Cirac, and P. Zoller, Quantum repeaters: The role of imperfect local operations in quantum communication, *Phys. Rev. Lett.* **81**, 5932 (1998).
 - [9] W. Dür, H.-J. Briegel, J. I. Cirac, and P. Zoller, Quantum repeaters based on entanglement purification, *Phys. Rev.*

- A **59**, 169 (1999).
- [10] S. D. Bartlett and W. J. Munro, Quantum teleportation of optical quantum gates, *Phys. Rev. Lett.* **90**, 117901 (2003).
- [11] K. S. Chou, J. Z. Blumoff, C. S. Wang, P. C. Reinhold, C. J. Axline, Y. Y. Gao, L. Frunzio, M. H. Devoret, L. Jiang, and R. J. Schoelkopf, Deterministic teleportation of a quantum gate between two logical qubits, *Nature* **561**, 368 (2018).
- [12] Y. Wan, D. Kienzler, S. D. Erickson, K. H. Mayer, T. R. Tan, J. J. Wu, H. M. Vasconcelos, S. Glancy, E. Knill, D. J. Wineland, A. C. Wilson, and D. Leibfried, Quantum gate teleportation between separated qubits in a trapped-ion processor, *Science* **364**, 875 (2019).
- [13] R. Raussendorf, D. E. Browne, and H. J. Briegel, Measurement-based quantum computation on cluster states, *Phys. Rev. A* **68**, 022312 (2003).
- [14] D. Gross and J. Eisert, Novel schemes for measurement-based quantum computation, *Phys. Rev. Lett.* **98**, 220503 (2007).
- [15] H. J. Briegel, D. E. Browne, W. Dür, R. Raussendorf, and M. Van den Nest, Measurement-based quantum computation, *Nature Physics* **5**, 19 (2009).
- [16] M. Studziński, S. Strelchuk, M. Mozrymas, and M. Horodecki, Port-based teleportation in arbitrary dimension, *Scientific reports* **7**, 10871 (2017).
- [17] K. Jeong, J. Kim, and S. Lee, Generalization of port-based teleportation and controlled teleportation capability, *Phys. Rev. A* **102**, 012414 (2020).
- [18] S. Pirandola, J. Eisert, C. Weedbrook, A. Furusawa, and S. L. Braunstein, Advances in quantum teleportation, *Nature Photonics* **9**, 641 (2015).
- [19] X.-M. Hu, Y. Guo, B.-H. Liu, C.-F. Li, and G.-C. Guo, Progress in quantum teleportation, *Nature Reviews Physics* **5**, 339 (2023).
- [20] I. Marcikic, H. De Riedmatten, W. Tittel, H. Zbinden, and N. Gisin, Long-distance teleportation of qubits at telecommunication wavelengths, *Nature* **421**, 509 (2003).
- [21] E. Lombardi, F. Sciarrino, S. Popescu, and F. De Martini, Teleportation of a vacuum-one-photon qubit, *Phys. Rev. Lett.* **88**, 070402 (2002).
- [22] A. Furusawa, J. L. Sørensen, S. L. Braunstein, C. A. Fuchs, H. J. Kimble, and E. S. Polzik, Unconditional quantum teleportation, *Science* **282**, 706 (1998).
- [23] S. Giacomini, F. Sciarrino, E. Lombardi, and F. De Martini, Active teleportation of a quantum bit, *Phys. Rev. A* **66**, 030302 (2002).
- [24] Y.-H. Kim, S. P. Kulik, and Y. Shih, Quantum teleportation of a polarization state with a complete bell state measurement, *Phys. Rev. Lett.* **86**, 1370 (2001).
- [25] D. Fattal, E. Diamanti, K. Inoue, and Y. Yamamoto, Quantum teleportation with a quantum dot single photon source, *Phys. Rev. Lett.* **92**, 037904 (2004).
- [26] S. Pirandola, J. Eisert, C. Weedbrook, A. Furusawa, and S. L. Braunstein, Advances in quantum teleportation, *Nature Photonics* **9**, 641 (2015).
- [27] X.-S. Ma, T. Herbst, T. Scheidl, D. Wang, S. Kropatschek, W. Naylor, B. Wittmann, A. Mech, J. Kofler, E. Anisimova, V. Makarov, T. Jennewein, R. Ursin, and A. Zeilinger, Quantum teleportation over 143 kilometres using active feed-forward, *Nature* **489**, 269 (2012).
- [28] J. Yin, J.-G. Ren, H. Lu, Y. Cao, H.-L. Yong, Y.-P. Wu, C. Liu, S.-K. Liao, F. Zhou, Y. Jiang, X.-D. Cai, P. Xu, G.-S. Pan, J.-J. Jia, Y.-M. Huang, H. Yin, J.-Y. Wang, Y.-A. Chen, C.-Z. Peng, and J.-W. Pan, Quantum teleportation and entanglement distribution over 100-kilometre free-space channels, *Nature* **488**, 185 (2012).
- [29] R. Valivarthi, M. G. Puigibert, Q. Zhou, G. H. Aguilar, V. B. Verma, F. Marsili, M. D. Shaw, S. W. Nam, D. Oblak, and W. Tittel, Quantum teleportation across a metropolitan fibre network, *Nature Photonics* **10**, 676 (2016).
- [30] F. Grosshans, Teleportation becomes streetwise, *Nature Photonics* **10**, 623 (2016).
- [31] S. Shen, C. Yuan, Z. Zhang, H. Yu, R. Zhang, C. Yang, H. Li, Z. Wang, Y. Wang, G. Deng, H. Song, L. You, Y. Fan, G. Guo, and Q. Zhou, Hertz-rate metropolitan quantum teleportation, *Light: Science & Applications* **12**, 115 (2023).
- [32] J.-G. Ren, P. Xu, H.-L. Yong, L. Zhang, S.-K. Liao, J. Yin, W.-Y. Liu, W.-Q. Cai, M. Yang, L. Li, K.-X. Yang, X. Han, Y.-Q. Yao, J. Li, H.-Y. Wu, S. Wan, L. Liu, D.-Q. Liu, Y.-W. Kuang, Z.-P. He, P. Shang, C. Guo, R.-H. Zheng, K. Tian, Z.-C. Zhu, N.-L. Liu, C.-Y. Lu, R. Shu, Y.-A. Chen, C.-Z. Peng, J.-Y. Wang, and J.-W. Pan, Ground-to-satellite quantum teleportation, *Nature* **549**, 70 (2017).
- [33] F. Basso Basset, M. B. Rota, C. Schimpf, D. Tedeschi, K. D. Zeuner, S. F. Covre da Silva, M. Reindl, V. Zwiller, K. D. Jöns, A. Rastelli, and R. Trotta, Entanglement swapping with photons generated on demand by a quantum dot, *Phys. Rev. Lett.* **123**, 160501 (2019).
- [34] W. P. Grice, Arbitrarily complete bell-state measurement using only linear optical elements, *Phys. Rev. A* **84**, 042331 (2011).
- [35] P. Senellart, G. Solomon, and A. White, High-performance semiconductor quantum-dot single-photon sources, *Nature Nanotechnology* **12**, 1026 (2017).
- [36] T. Heindel, J.-H. Kim, N. Gregersen, A. Rastelli, and S. Reitzenstein, Quantum dots for photonic quantum information technology, *Adv. Opt. Photon.* **15**, 613 (2023).
- [37] Y. Arakawa and M. J. Holmes, Progress in quantum-dot single photon sources for quantum information technologies: A broad spectrum overview, *Applied Physics Reviews* **7**, 021309 (2020).
- [38] N. Somaschi, V. Giesz, L. De Santis, J. Loredó, M. P. Almeida, G. Hornecker, S. L. Portalupi, T. Grange, C. Antón, J. Demory, C. Gomez, I. Sagnes, N. D. Lanzillotti-Kimura, A. Lemaitre, A. Auffèves, A. G. White, L. Lanco, and P. Senellart, Near-optimal single-photon sources in the solid state, *Nature Photonics* **10**, 340 (2016).
- [39] C.-Y. Lu and J.-W. Pan, Quantum-dot single-photon sources for the quantum internet, *Nature Nanotechnology* **16**, 1294 (2021).
- [40] F. Basso Basset, M. Valeri, E. Roccia, V. Muredda, D. Poderini, J. Neuwirth, N. Spagnolo, M. B. Rota, G. Carvacho, F. Sciarrino, and R. Trotta, Quantum key distribution with entangled photons generated on demand by a quantum dot, *Science Advances* **7**, eabe6379 (2021).
- [41] H. Cao, L. M. Hansen, F. Giorgino, L. Carosini, P. Zakhalka, F. Zilk, J. C. Loredó, and P. Walther, A photonic source of heralded ghz states (2023), [arXiv:2308.05709](https://arxiv.org/abs/2308.05709) [quant-ph].
- [42] N. Maring, A. Fyrillas, M. Pont, E. Ivanov, P. Stepanov, N. Margaria, W. Hease, A. Pishchagin, T. H. Au,

- S. Boissier, E. Bertasi, A. Baert, M. Valdivia, M. Billard, O. Acar, A. Brioussel, R. Mezher, S. C. Wein, A. Salavrakos, P. Sinnott, D. A. Fioretto, P.-E. Emery, N. Belabas, S. Mansfield, P. Senellart, J. Senellart, and N. Somaschi, A general-purpose single-photon-based quantum computing platform (2023), [arXiv:2306.00874 \[quant-ph\]](#).
- [43] S. Chen, L.-C. Peng, Y.-P. Guo, X.-M. Gu, X. Ding, R.-Z. Liu, X. You, J. Qin, Y.-F. Wang, Y.-M. He, J. J. Renema, Y.-H. Huo, H. Wang, C.-Y. Lu, and J.-W. Pan, Heralded three-photon entanglement from a single-photon source on a photonic chip (2023), [arXiv:2307.02189 \[quant-ph\]](#).
- [44] H. Wang, Y.-M. He, T.-H. Chung, H. Hu, Y. Yu, S. Chen, X. Ding, M.-C. Chen, J. Qin, X. Yang, R.-Z. Liu, Z.-C. Duan, J.-P. Li, S. Gerhardt, K. Winkler, J. Jurkat, L.-J. Wang, N. Gregersen, Y.-H. Huo, Q. Dai, S. Yu, S. Höfling, C.-Y. Lu, and J.-W. Pan, Towards optimal single-photon sources from polarized microcavities, *Nature Photonics* **13**, 770 (2019).
- [45] J. Loredó, C. Antón, B. Reznichenko, P. Hilaire, A. Harouri, C. Millet, H. Ollivier, N. Somaschi, L. De Santis, A. Lemaître, I. Sagnes, L. Lanco, A. Auffèves, O. Krebs, and P. Senellart, Generation of non-classical light in a photon-number superposition, *Nature Photonics* **13**, 803 (2019).
- [46] S. C. Wein, J. C. Loredó, M. Maffei, P. Hilaire, A. Harouri, N. Somaschi, A. Lemaître, I. Sagnes, L. Lanco, O. Krebs, A. Auffèves, C. Simon, P. Senellart, and C. Antón-Solanas, Photon-number entanglement generated by sequential excitation of a two-level atom, *Nature Photonics* **16**, 374 (2022).
- [47] H.-W. Lee and J. Kim, Quantum teleportation and bell's inequality using single-particle entanglement, *Phys. Rev. A* **63**, 012305 (2000).
- [48] S. Massar and S. Popescu, Optimal extraction of information from finite quantum ensembles, *Phys. Rev. Lett.* **74**, 1259 (1995).
- [49] J. J. Renema, Simulability of partially distinguishable superposition and gaussian boson sampling, *Phys. Rev. A* **101**, 063840 (2020).
- [50] F. Flamini, N. Spagnolo, and F. Sciarrino, Photonic quantum information processing: a review, *Rep. Prog. Phys.* **82**, 016001 (2018).
- [51] Ö. Erkiş, L. Conlon, B. Shajilal, S. Kish, S. Tserkis, Y.-S. Kim, P. K. Lam, and S. M. Assad, Surpassing the repeaterless bound with a photon-number encoded measurement-device-independent quantum key distribution protocol, *npj Quantum Information* **9**, 29 (2023).
- [52] Y. Karli, D. A. Vajner, F. Kappe, P. C. A. Hagen, L. M. Hansen, R. Schwarz, T. K. Bracht, C. Schimpf, S. F. C. da Silva, P. Walther, A. Rastelli, V. M. Axt, J. C. Loredó, V. Remesh, T. Heindel, D. E. Reiter, and G. Weihs, Controlling the photon number coherence of solid-state quantum light sources for quantum cryptography (2023), [arXiv:2305.20017 \[quant-ph\]](#).

Supplementary Information: Quantum teleportation of a genuine vacuum–one-photon qubit generated via a quantum dot source

Beatrice Polacchi,¹ Francesco Hoch,¹ Giovanni Rodari,¹ Stefano Savo,¹
Gonzalo Carvacho,¹ Nicolò Spagnolo,¹ Taira Giordani,^{1,*} and Fabio Sciarrino¹

¹*Dipartimento di Fisica - Sapienza Università di Roma, P.le Aldo Moro 5, I-00185 Roma, Italy*

I. CHARACTERIZATION OF THE PROBE STATE VIA SELF-HOMODYNING IN A MACH-ZEHNDER INTERFEROMETER

In this Section, we describe how the vacuum population of our target states is formally linked to their measured fringe visibility when measured in a time-unbalanced MZI. These results will allow us to extrapolate the purity of the states generated by our source, as well as to find the relationship between the target state visibility V_S and the visibility of the teleported state V_T , as reported in the next section.

We start by considering the quantum state entering the MZI, which is composed, in principle, by a train of n photon states. However, due to the losses in our setup, mainly caused by a low source extraction ($\approx 10\%$) and detection efficiency ($\approx 30\%$), we map the interferometer of Fig. 2b in the main text as if two states were impinging on a beam splitter, with high losses at the output. Under these assumptions, the input state becomes:

$$|\psi_b\rangle = \left(\alpha + \beta a_1^\dagger\right) \left(\alpha + \beta e^{i\phi} a_2^\dagger\right) |0\rangle. \quad (1)$$

After the beam splitter, the state evolves into:

$$|\psi_{\text{out}}\rangle = \left(\alpha + \beta \frac{a_1^\dagger + a_2^\dagger}{\sqrt{2}}\right) \left(\alpha + \beta e^{i\phi} \frac{a_1^\dagger - a_2^\dagger}{\sqrt{2}}\right) |0\rangle = \left[\alpha^2 + \frac{\alpha\beta(1+e^{i\phi})}{\sqrt{2}} a_1^\dagger + \frac{\alpha\beta(1-e^{i\phi})}{\sqrt{2}} a_2^\dagger + \frac{\beta^2 e^{i\phi}}{2} (a_1^{\dagger 2} - a_2^{\dagger 2})\right] |0\rangle. \quad (2)$$

Considering that in a threshold detector a single photon has probability η to be detected, while two-photon inputs trigger the detector with probability $1 - (1 - \eta)^2$, we find that detector on output port 1 clicks with overall probability:

$$P_1(\phi) = \eta \frac{|\alpha|^2 |\beta|^2}{2} (2 + 2 \cos \phi) + \frac{|\beta|^2}{4} 2[\eta^2 + 2\eta(1 - \eta)] = \frac{\eta\beta^2}{2} (2 - |\beta|^2 \eta + 2|\alpha|^2 \cos \phi), \quad (3)$$

being η the overall loss parameter. By defining the visibility of the fringe pattern as:

$$V = \frac{\max_\phi P_1(\phi) - \min_\phi P_1(\phi)}{\max_\phi P_1(\phi) + \min_\phi P_1(\phi)}, \quad (4)$$

we find that, in the limit of high losses, ($\eta \rightarrow 0$) the visibility is:

$$V = |\alpha|^2. \quad (5)$$

This result can be extended to include partial photon distinguishability between the photon modes. This is obtained by considering an input state of the form:

$$|\psi_b^{x_1, x_2}\rangle = \left(\alpha + \beta \sqrt{x_A} a_1^\dagger + \beta \sqrt{1 - x_A} b_1^\dagger\right) \left(\alpha + \beta e^{i\phi} \sqrt{x_B} a_2^\dagger + \beta e^{i\phi} \sqrt{1 - x_B} c_2^\dagger\right) |0\rangle, \quad (6)$$

where b_1^\dagger and c_2^\dagger are two additional fictitious modes, mutually orthogonal and orthogonal to $(a_1^\dagger, a_2^\dagger)$, that are used to model the effect of partially distinguishability due to the photon internal degrees of freedom. Parameters (x_A, x_B) are related to the Hong-Ou-Mandel visibility between the two photons as $V_{\text{HOM}} = x_A x_B$. Moreover, we include the purity of the state generated by the source. Indeed, each of the two states impinging on the beam splitter can be modeled as follows:

$$\rho_s = \lambda \rho_{\text{pure}} + (1 - \lambda) \rho_{\text{mixed}} \quad (7)$$

* taira.giordani@uniroma1.it

where ρ_{pure} is the density matrix associated to a pure state input [see Eq. (1) in the main text], and $\rho_{\text{mixed}} = |\alpha|^2 |0\rangle\langle 0| + |\beta|^2 |1\rangle\langle 1|$. By repeating the calculation above, and by tracing over the internal degrees of freedom of the photons, the fringe visibility of the state at the output of the interferometer is found to be $V = \lambda^2 \sqrt{x_A x_B} |\alpha|^2$. By using the notation of the main text ($\alpha = \alpha_S$), we finally obtain:

$$V_S = \lambda^2 \sqrt{V_{\text{HOM}}^{\text{Alice}}} |\alpha_S|^2 \quad (8)$$

This relationship can be employed to λ , from the linear fit reported in the inset of Fig. 3a of the main text. Indeed, by considering also the high loss regime, the measured signal rate is proportional to:

$$S_c \propto \langle P_1(\phi) \rangle_\phi \propto (1 - \alpha_S^2) \quad (9)$$

which means that the visibility V_S is by itself linearly proportional to S_c , with slope dependent from the purity λ .

II. FULL MODEL OF THE TELEPORTATION SCHEME

In this section, we develop a model to describe the expected visibility of states teleported with our platform, V_T , and discuss its relationship with the visibility of the target state V_S . We will refer to the spatial modes, to the beam-splitters (BS), and to the delay loops as labeled in Fig. 1.

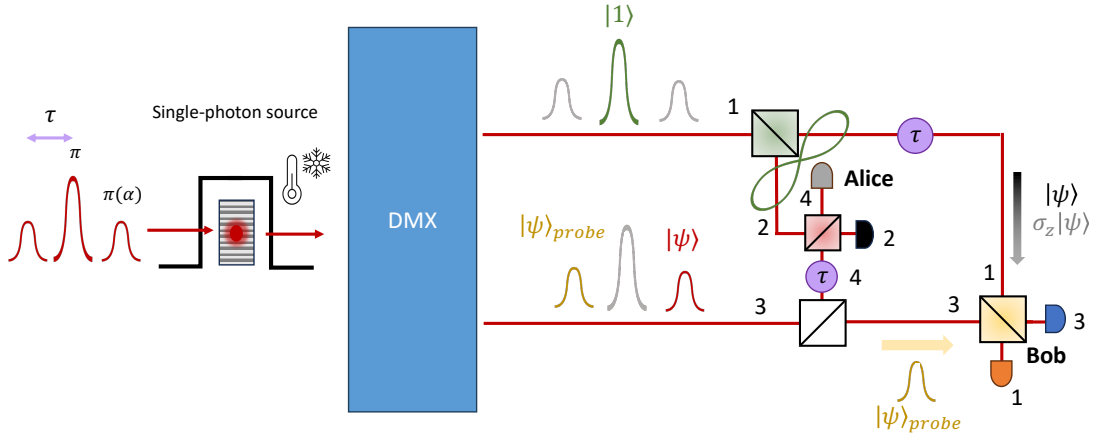


Figure 1. **Teleportation scheme.** Here we recall the teleportation scheme, already reported in the main text, by adding the modes labels used for the calculations carried out in this section.

We first consider an initial state where partial photon indistinguishability is not included, as:

$$|\psi\rangle_{3,2\tau} \otimes |1\rangle_{1,\tau} \otimes |\psi\rangle_{3,0} = (\alpha |0\rangle + \beta |1\rangle)_{3,2\tau} \otimes |1\rangle_{1,\tau} \otimes (\alpha |0\rangle + \gamma |1\rangle)_{3,0} = (\alpha + \beta a_{3,2\tau}^\dagger) a_{1,\tau}^\dagger (\alpha + \gamma a_{3,0}^\dagger) |0\rangle, \quad (10)$$

where $\gamma = |\beta|e^{i\chi}$, $\beta = |\beta|e^{i\phi}$ and $\phi - \chi = \delta$.

After application of BS_{12} the state evolves into:

$$(\alpha + \beta a_{3,2\tau}^\dagger) \frac{1}{\sqrt{2}} (a_{1,\tau}^\dagger + a_{2,\tau}^\dagger) (\alpha + \gamma a_{3,0}^\dagger) |0\rangle. \quad (11)$$

Then, after application of BS_{34} we find:

$$\left(\alpha + \beta \frac{a_{3,2\tau}^\dagger + a_{4,2\tau}^\dagger}{\sqrt{2}} \right) \frac{1}{\sqrt{2}} (a_{1,\tau}^\dagger + a_{2,\tau}^\dagger) \left(\alpha + \gamma \frac{a_{3,0}^\dagger + a_{4,0}^\dagger}{\sqrt{2}} \right) |0\rangle. \quad (12)$$

After application of delay τ on mode 4 we obtain:

$$\left(\alpha + \beta \frac{a_{3,2\tau}^\dagger + a_{4,3\tau}^\dagger}{\sqrt{2}} \right) \frac{1}{\sqrt{2}} (a_{1,\tau}^\dagger + a_{2,\tau}^\dagger) \left(\alpha + \gamma \frac{a_{3,0}^\dagger + a_{4,\tau}^\dagger}{\sqrt{2}} \right) |0\rangle \quad (13)$$

After application of BS_{24} , we find:

$$\left(\alpha + \frac{\beta}{2}(\sqrt{2}a_{3,2\tau}^\dagger + a_{2,3\tau}^\dagger - a_{4,3\tau}^\dagger)\right) \frac{1}{2} \left(\sqrt{2}a_{1,\tau}^\dagger + a_{2,\tau}^\dagger + a_{4,\tau}^\dagger\right) \left(\alpha + \frac{\gamma}{2}(\sqrt{2}a_{3,0}^\dagger + a_{2,\tau}^\dagger - a_{4,\tau}^\dagger)\right) |0\rangle. \quad (14)$$

After application of delay τ on mode 1 we obtain:

$$\left(\alpha + \frac{\beta}{2}(\sqrt{2}a_{3,2\tau}^\dagger + a_{2,3\tau}^\dagger - a_{4,3\tau}^\dagger)\right) \frac{1}{2} \left(\sqrt{2}a_{1,2\tau}^\dagger + a_{2,\tau}^\dagger + a_{4,\tau}^\dagger\right) \left(\alpha + \frac{\gamma}{2}(\sqrt{2}a_{3,0}^\dagger + a_{2,\tau}^\dagger - a_{4,\tau}^\dagger)\right) |0\rangle. \quad (15)$$

Finally, after application of BS_{13} the state can be written as:

$$\left[\alpha + \frac{\beta}{2}(a_{3,2\tau}^\dagger + a_{1,2\tau}^\dagger + a_{2,3\tau}^\dagger - a_{4,3\tau}^\dagger)\right] \frac{1}{2} \left(a_{3,2\tau}^\dagger - a_{1,2\tau}^\dagger + a_{2,\tau}^\dagger + a_{4,\tau}^\dagger\right) \left[\alpha + \frac{\gamma}{2}(a_{3,0}^\dagger + a_{1,0}^\dagger + a_{2,\tau}^\dagger - a_{4,\tau}^\dagger)\right] |0\rangle. \quad (16)$$

The output state at the detection can be also rearranged as:

$$\begin{aligned} & \frac{\alpha^2}{2} \left[a_{3,2\tau}^\dagger - a_{1,2\tau}^\dagger + a_{2,\tau}^\dagger - a_{4,\tau}^\dagger \right] + \frac{\alpha\gamma}{4} \left[\left(a_{3,2\tau}^\dagger - a_{1,2\tau}^\dagger \right) \left(a_{3,0}^\dagger + a_{1,0}^\dagger \right) + \left(a_{3,2\tau}^\dagger - a_{1,2\tau}^\dagger \right) \left(a_{2,\tau}^\dagger - a_{4,\tau}^\dagger \right) + \right. \\ & + \left. \left(a_{2,\tau}^\dagger + a_{4,\tau}^\dagger \right) \left(a_{3,0}^\dagger + a_{1,0}^\dagger \right) + \left(a_{2,\tau}^\dagger + a_{4,\tau}^\dagger \right) \left(a_{2,\tau}^\dagger - a_{4,\tau}^\dagger \right) \right] + \frac{\alpha\beta}{4} \left[\left(a_{3,2\tau}^\dagger + a_{1,2\tau}^\dagger \right) \left(a_{3,2\tau}^\dagger - a_{1,2\tau}^\dagger \right) + \right. \\ & + \left. \left(a_{2,3\tau}^\dagger - a_{4,3\tau}^\dagger \right) \left(a_{2,\tau}^\dagger + a_{4,\tau}^\dagger \right) + \left(a_{3,2\tau}^\dagger + a_{1,2\tau}^\dagger \right) \left(a_{2,\tau}^\dagger + a_{4,\tau}^\dagger \right) + \left(a_{2,3\tau}^\dagger - a_{4,3\tau}^\dagger \right) \left(a_{3,2\tau}^\dagger - a_{1,2\tau}^\dagger \right) \right] + \\ & + \frac{\beta\gamma}{8} \left[\left(a_{3,2\tau}^\dagger + a_{1,2\tau}^\dagger \right) \left(a_{3,2\tau}^\dagger - a_{1,2\tau}^\dagger \right) \left(a_{3,0}^\dagger + a_{1,0}^\dagger \right) + \left(a_{3,2\tau}^\dagger + a_{1,2\tau}^\dagger \right) \left(a_{3,2\tau}^\dagger - a_{1,2\tau}^\dagger \right) \left(a_{2,\tau}^\dagger - a_{4,\tau}^\dagger \right) + \right. \\ & + \left. \left(a_{3,2\tau}^\dagger + a_{1,2\tau}^\dagger \right) \left(a_{2,\tau}^\dagger + a_{4,\tau}^\dagger \right) \left(a_{3,0}^\dagger + a_{1,0}^\dagger \right) + \left(a_{3,2\tau}^\dagger + a_{1,2\tau}^\dagger \right) \left(a_{2,\tau}^\dagger + a_{4,\tau}^\dagger \right) \left(a_{2,\tau}^\dagger - a_{4,\tau}^\dagger \right) + \right. \\ & + \left. \left(a_{2,3\tau}^\dagger - a_{4,3\tau}^\dagger \right) \left(a_{3,2\tau}^\dagger - a_{1,2\tau}^\dagger \right) \left(a_{3,0}^\dagger + a_{1,0}^\dagger \right) + \left(a_{2,3\tau}^\dagger - a_{4,3\tau}^\dagger \right) \left(a_{3,2\tau}^\dagger - a_{1,2\tau}^\dagger \right) \left(a_{2,\tau}^\dagger - a_{4,\tau}^\dagger \right) + \right. \\ & + \left. \left(a_{2,3\tau}^\dagger - a_{4,3\tau}^\dagger \right) \left(a_{2,\tau}^\dagger + a_{4,\tau}^\dagger \right) \left(a_{3,0}^\dagger + a_{1,0}^\dagger \right) + \left(a_{2,3\tau}^\dagger - a_{4,3\tau}^\dagger \right) \left(a_{2,\tau}^\dagger + a_{4,\tau}^\dagger \right) \left(a_{2,\tau}^\dagger - a_{4,\tau}^\dagger \right) \right] |0\rangle. \quad (17) \end{aligned}$$

From this expression, we can now the probability of having an event where one detector per station clicks. More specifically, we need to consider coincidences event between one detector of the pair (1,3), clicking at time 2τ , and one detector of the pair (2,4), clicking at time τ . The four combinations for all probabilities are found to be:

$$\begin{aligned} P(1, 2) &= \frac{|\beta|^2}{16} (2 - 2|\alpha|^2 \cos \delta), \\ P(1, 4) &= \frac{|\beta|^2}{16} (2 + 2|\alpha|^2 \cos \delta), \\ P(3, 2) &= \frac{|\beta|^2}{16} (2 + 2|\alpha|^2 \cos \delta), \\ P(3, 4) &= \frac{|\beta|^2}{16} (2 - 2|\alpha|^2 \cos \delta), \end{aligned} \quad (18)$$

leading to the following visibility:

$$V_T = |\alpha|^2 \quad (19)$$

Analogously to the previous section, we need to consider the different effects due to the experimental implementation, that is, losses, purity and partial photon indistinguishability. We begin by including the effect of losses in our setup, analogously to the derivation above. Since the loss operator commutes with the other operators, we can compute the teleported visibility in a lossy platform, by considering all losses placed at the output. So, with respect to the previous derivation, the probabilities of the interesting events become:

$$\begin{aligned} P(1_{2\tau}, 2_\tau) &= \frac{|\beta|^2 \eta_1 \eta_2}{32} (6 - \eta_1 - \eta_2 - (2 - \eta_1 - \eta_2)|\alpha|^2 - 4|\alpha|^2 \cos \delta), \\ P(1_{2\tau}, 4_\tau) &= \frac{|\beta|^2 \eta_1 \eta_4}{32} (6 - \eta_1 - \eta_4 - (2 - \eta_1 - \eta_4)|\alpha|^2 + 4|\alpha|^2 \cos \delta), \\ P(3_{2\tau}, 2_\tau) &= \frac{|\beta|^2 \eta_3 \eta_2}{32} (6 - \eta_3 - \eta_2 - (2 - \eta_3 - \eta_2)|\alpha|^2 + 4|\alpha|^2 \cos \delta), \\ P(3_{2\tau}, 4_\tau) &= \frac{|\beta|^2 \eta_3 \eta_4}{32} (6 - \eta_3 - \eta_4 - (2 - \eta_3 - \eta_4)|\alpha|^2 - 4|\alpha|^2 \cos \delta), \end{aligned} \quad (20)$$

where $\eta_1 \dots \eta_4$ are the detection probabilities at the four outputs. In the limit $\eta_i \rightarrow 0$, all probabilities have the same visibility which is found to be:

$$V_T = \frac{2|\alpha|^2}{3 - |\alpha|^2}. \quad (21)$$

Finally, with analogous procedure to the one discussed in the previous section, we now take into account also the state non-ideal purity $\lambda < 1$ and HOM visibilities. By considering the notation $\alpha = \alpha_T$ for the teleported state, we find that the previous formula becomes:

$$V_T = \frac{2\lambda^2 \sqrt{V_{\text{HOM}}^{\text{Alice}} V_{\text{HOM}}^{\text{Bob}} |\alpha_T|^2}}{3 - |\alpha_T|^2}. \quad (22)$$

In this way, the relationship between the target state visibility V_S and the teleported visibility V_T in our platform by considering $\alpha_S = \alpha_T$ can be written as:

$$V_T = \frac{2\lambda^2 \sqrt{V_{\text{HOM}}^{\text{Alice}} V_{\text{HOM}}^{\text{Bob}} V_S}}{3\lambda^2 \sqrt{V_{\text{HOM}}^{\text{Alice}} - V_S}}. \quad (23)$$

This expression has been used as the green line in Fig. 3a of the main text to identify the expected visibility from the collected experimental data. The experimental values of the target state visibilities and vacuum populations, and teleported visibilities, are reported in Table I.

$ \alpha_S ^2$	V_S	V_T
0.211 ± 0.001	0.197 ± 0.001	0.13 ± 0.02
0.323 ± 0.005	0.303 ± 0.005	0.21 ± 0.02
0.425 ± 0.002	0.398 ± 0.002	0.26 ± 0.02
0.545 ± 0.006	0.510 ± 0.006	0.36 ± 0.03
0.632 ± 0.004	0.591 ± 0.004	0.41 ± 0.04
0.769 ± 0.005	0.720 ± 0.005	0.52 ± 0.05

Table I. Comparison between the visibility of the teleported state V_T with the visibility of the target state V_S with vacuum population $|\alpha_S|^2$, estimated independently via the self-homodyning procedure in a MZI.

III. ESTIMATION OF THE VISIBILITY

In this section, we report the derivation of a reliable procedure that we employed to estimate the fringe visibility. As discussed here, such a method allows an accurate estimation of the visibility of a single-count trace even in the presence of low statistics, whereas standard methods would significantly overestimate it, as depicted in Fig. 2. A single-count time trace can be expressed as:

$$n(t) = \mathcal{P} \left(N \frac{1 + V \cos(\phi(t))}{2} \right) \quad (24)$$

where $\mathcal{P}(\cdot)$ is a sample from a Poissonian distribution with mean value equal to the quantity in the parenthesis, $\phi(t)$ is a stochastic variable that varies slowly compared to signal sampling times, N is the average number of photons and V is the fringes visibility of the signal that is the parameter to be estimated.

The standard procedure to measure the visibility of a single-count trace, as the one in Eq. (24), consists of applying the following formula:

$$V = \frac{\max(n(t)) - \min(n(t))}{\max(n(t)) + \min(n(t))} \quad (25)$$

but, as shown in Fig. 2a, if the number of photons N is small, then a significant bias is obtained in the estimation of the visibility, especially in the region of the teleportation and entanglement swapping experiments (that is, $N = 10^0 \div 10^2$, highlighted in yellow in the figure).

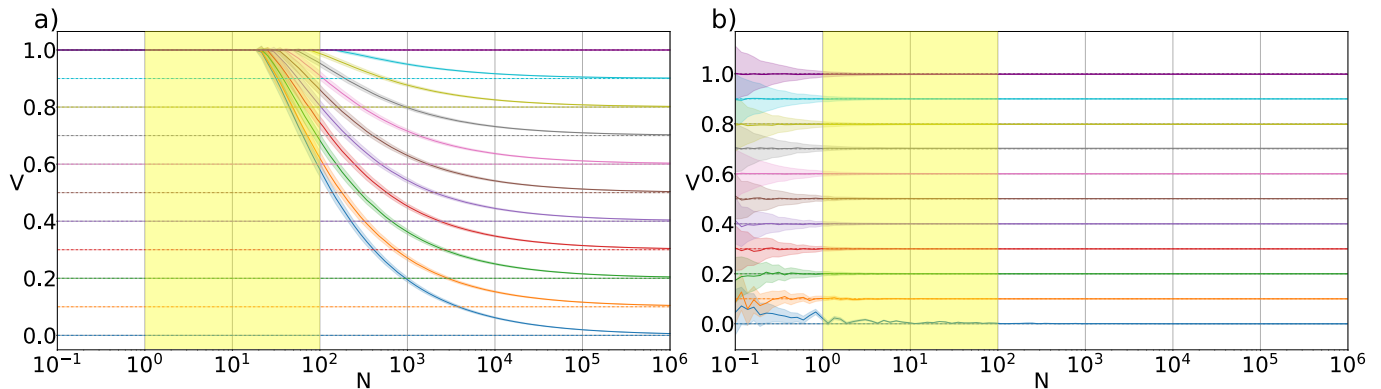


Figure 2. **Estimation of fringes visibility.** Numerical simulation of the visibility measurement for a typical time trace of the experiment that covers 10^5 time bins of 50ms, as a function of the average number of photons N in each time bin. The dashed line represents the true visibility of the fringes. The solid line is the mean value reconstructed by averaging on 1000 instances of the simulation. The shaded regions represent the variance of such estimations. In a) the visibility is estimated according to Eq. (25); b) represents the reconstruction based on the measure of the trace variance. The region highlighted in yellow is the range of the N in our teleportation experiment.

To overcome this issue, we employed a different approach based on the measurement of the signal variance. Under the reasonable assumption that $\langle \cos(\phi(t)) \rangle_t = 0$ and $\langle \cos(2\phi(t)) \rangle_t = 0$, and that the time trace is sufficiently long and hence statistically significant, then we can compute the time average of the signal and of the square of the signal as:

$$\langle n \rangle_t = \left\langle N \frac{1 + V \cos(\phi(t))}{2} \right\rangle = \frac{N}{2} \quad (26)$$

$$\langle n^2 \rangle_t = \left\langle \left(N \frac{1 + V \cos(\phi(t))}{2} \right)^2 \right\rangle + \left\langle N \frac{1 + V \cos(\phi(t))}{2} \right\rangle = \frac{N^2}{4} \left(1 + \frac{V^2}{2} \right) + \frac{N}{2} \quad (27)$$

By combining previous equations we obtain:

$$V^2 = 2 \frac{\langle n^2 \rangle_t - \langle n \rangle_t^2 - \langle n \rangle_t}{\langle n \rangle_t^2} \quad (28)$$

As we can observe, in Fig. 2b this approach is more reliable compared to the previous one, due to the fast convergence of the estimated value of the visibility in the regime of the low values of N , i.e. of low statistics.

IV. FULL MODEL OF THE ENTANGLEMENT SWAPPING EXPERIMENT

In this section, we derive the model employed to describe the expected visibility of the output state after the entanglement swapping protocol. In this derivation, we first consider the case where the two interfering states are two single-photon states, and the BS transmittance is $T = 0.5$. Then, we will consider a noise model where the states at the input are allowed to have a nonzero vacuum component. We refer to Fig. 3 for mode labelling and for the sequence of operations considered in the model.

A. Single-photon input case

We consider here the ideal case where all BS in Fig. 3 have transmittance $t_i^2 = T_i = 0.5$, and the input state is a set of two single photons:

$$|1\rangle_\tau |1\rangle_0. \quad (29)$$

Such a state can be written through creation operators as:

$$\left[a_{1,\tau}^\dagger \right] \left[a_{1,0}^\dagger \right] |0\rangle. \quad (30)$$

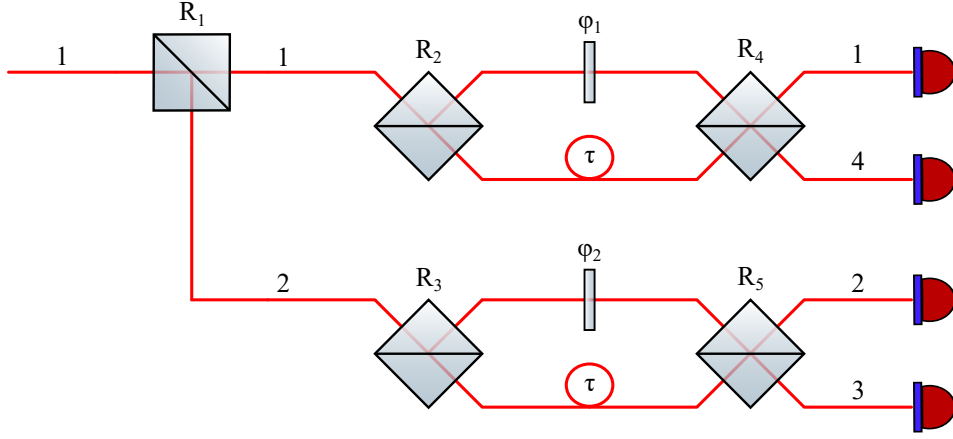


Figure 3. **Entanglement swapping apparatus.** Scheme of the optical modes and beam-splitters reflectivities ($R_i = 1 - T_i$) to perform the entanglement swapping.

After propagation through the first BS, that acts as $a_1^\dagger \rightarrow (a_1^\dagger + a_2^\dagger)/\sqrt{2}$, the state becomes:

$$\frac{1}{2} [a_{1,\tau}^\dagger + a_{2,\tau}^\dagger] [a_{1,0}^\dagger + a_{2,0}^\dagger] |0\rangle. \quad (31)$$

Then, after the first layer of two BS evolutions, the state will evolve into:

$$\frac{1}{4} [a_{1,\tau}^\dagger + a_{4,\tau}^\dagger + a_{3,\tau}^\dagger + a_{2,\tau}^\dagger] [a_{1,0}^\dagger + a_{4,0}^\dagger + a_{3,0}^\dagger + a_{2,0}^\dagger] |0\rangle. \quad (32)$$

Before the last layer of two BSs, we observe that:

- mode 1 and 2 will acquire a time delay equal to τ ;
- mode 4 and mode 3 will acquire a relative phase shift $e^{i\phi}$ and $e^{i\phi'}$ respectively, due to the propagation in the Mach-Zehnder interferometer.

The state before the final layer of BSs becomes:

$$\frac{1}{4} [a_{1,2\tau}^\dagger + e^{i\phi} a_{4,\tau}^\dagger + e^{i\phi'} a_{3,\tau}^\dagger + a_{2,2\tau}^\dagger] [a_{1,\tau}^\dagger + e^{i\phi} a_{4,0}^\dagger + e^{i\phi'} a_{3,0}^\dagger + a_{2,\tau}^\dagger] |0\rangle. \quad (33)$$

By looking at a specific time bin $t = \tau$, we can neglect the other terms and keep only the following part of the state:

$$\frac{1}{4} [e^{i\phi} a_{4,\tau}^\dagger + e^{i\phi'} a_{3,\tau}^\dagger] [a_{1,\tau}^\dagger + a_{2,\tau}^\dagger] |0\rangle. \quad (34)$$

By applying the evolution of the final layer of two BSs, we obtain that the relevant part of the final state reads:

$$\frac{1}{8} [e^{i\phi} a_{4,\tau}^\dagger + e^{i\phi} a_{1,\tau}^\dagger + e^{i\phi'} a_{2,\tau}^\dagger - e^{i\phi'} a_{3,\tau}^\dagger] [a_{4,\tau}^\dagger - a_{1,\tau}^\dagger + a_{2,\tau}^\dagger + a_{3,\tau}^\dagger] |0\rangle. \quad (35)$$

The probabilities $P_{4,2}$, $P_{4,3}$, $P_{1,2}$, $P_{1,3}$ for the relevant two-fold coincidence events $CC_{4,2}$, $CC_{4,3}$, $CC_{1,2}$, $CC_{1,3}$, can be then obtained as:

$$P_{1,2}^{\text{ID}} = \frac{1}{32} (1 - \cos\xi); \quad P_{1,3}^{\text{ID}} = \frac{1}{32} (1 + \cos\xi); \quad P_{4,2}^{\text{ID}} = \frac{1}{32} (1 + \cos\xi); \quad P_{4,3}^{\text{ID}} = \frac{1}{32} (1 - \cos\xi). \quad (36)$$

where $\xi = \phi - \phi'$. In this ideal scenario, all visibilities are then equal to 1.

B. Model of the experiment

We now consider the scenario where the two states contain a small superposition with a vacuum component. The input state is then written as:

$$[\alpha |0\rangle + \beta |1\rangle]_\tau [\alpha |0\rangle + \gamma |1\rangle]_0, \quad (37)$$

where γ is related to β through a phase shift $\gamma = e^{i\delta}\beta$. Expressing the one-photon state through the creation operators, the initial state is written as:

$$\left[\alpha + \beta a_{1,\tau}^\dagger \right] \left[\alpha + \gamma a_{1,0}^\dagger \right] |0\rangle. \quad (38)$$

We then follow the same assumptions of the ideal case, except that the transmittance of the BSs can be different than 0.5. Therefore, the first BS would transform the creation operators as $a_1^\dagger \rightarrow (t_1 a_1^\dagger + r_1 a_2^\dagger)$, and the state becomes:

$$\left[\alpha + \beta (t_1 a_{1,\tau}^\dagger + r_1 a_{2,\tau}^\dagger) \right] \left[\alpha + \gamma (t_1 a_{1,0}^\dagger + r_1 a_{2,0}^\dagger) \right] |0\rangle. \quad (39)$$

Then, by considering the evolution induced by BS₂ and BS₃, we obtain the following state:

$$\left[\alpha + \beta t_1 (t_2 a_{1,\tau}^\dagger + r_2 a_{4,\tau}^\dagger) + \beta r_1 (r_3 a_{3,\tau}^\dagger + t_3 a_{2,\tau}^\dagger) \right] \left[\alpha + \gamma t_1 (t_2 a_{1,0}^\dagger + r_2 a_{4,0}^\dagger) + \gamma r_1 (r_3 a_{3,0}^\dagger + t_3 a_{2,0}^\dagger) \right] |0\rangle, \quad (40)$$

that can be also expanded:

$$\left[\alpha + \beta t_1 t_2 a_{1,\tau}^\dagger + \beta t_1 r_2 a_{4,\tau}^\dagger + \beta r_1 r_3 a_{3,\tau}^\dagger + \beta r_1 t_3 a_{2,\tau}^\dagger \right] \left[\alpha + \gamma t_1 t_2 a_{1,0}^\dagger + \gamma t_1 r_2 a_{4,0}^\dagger + \gamma r_1 r_3 a_{3,0}^\dagger + \gamma r_1 t_3 a_{2,0}^\dagger \right] |0\rangle. \quad (41)$$

As for the previous calculations, we have that:

- mode 1 and 2 will acquire a time delay equal to τ ;
- mode 4 and mode 3 will acquire a relative phase shift $e^{i\phi}$ and $e^{i\phi'}$ respectively, due to the propagation in the Mach-Zehnder interferometer.

Hence, the state evolves into:

$$\begin{aligned} & \left[\alpha + \beta t_1 t_2 a_{1,2\tau}^\dagger + e^{i\phi} \beta t_1 r_2 a_{4,\tau}^\dagger + e^{i\phi'} \beta r_1 r_3 a_{3,\tau}^\dagger + \beta r_1 t_3 a_{2,2\tau}^\dagger \right] \times \\ & \times \left[\alpha + \gamma t_1 t_2 a_{1,\tau}^\dagger + e^{i\phi} \gamma t_1 r_2 a_{4,0}^\dagger + e^{i\phi'} \gamma r_1 r_3 a_{3,0}^\dagger + \gamma r_1 t_3 a_{2,\tau}^\dagger \right] |0\rangle. \end{aligned} \quad (42)$$

By keeping only terms related to time bin $t = \tau$, and by neglecting the vacuum components that will not lead to a useful two-fold coincidence events, we can write the relevant portion of the state as:

$$\left[e^{i\phi} \beta t_1 r_2 a_{4,\tau}^\dagger + e^{i\phi'} \beta r_1 r_3 a_{3,\tau}^\dagger \right] \left[\gamma t_1 t_2 a_{1,\tau}^\dagger + \gamma r_1 t_3 a_{2,\tau}^\dagger \right] |0\rangle. \quad (43)$$

After the evolution of the final layer of two BSs, the relevant part of the final state reads:

$$\begin{aligned} & \left[e^{i\phi} \beta t_1 r_2 r_4 a_{1,\tau}^\dagger + e^{i\phi} \beta t_1 r_2 t_4 a_{4,\tau}^\dagger + e^{i\phi'} \beta r_1 r_3 r_5 a_{2,\tau}^\dagger - e^{i\phi'} \beta r_1 r_3 t_5 a_{3,\tau}^\dagger \right] \times \\ & \times \left[\gamma t_1 t_2 r_4 a_{4,\tau}^\dagger - \gamma t_1 t_2 t_4 a_{1,\tau}^\dagger + \gamma r_1 t_3 t_5 a_{2,\tau}^\dagger + \gamma r_1 t_3 r_5 a_{3,\tau}^\dagger \right] |0\rangle. \end{aligned} \quad (44)$$

We can now obtain the probabilities $P_{4,2}$, $P_{4,3}$, $P_{1,2}$, $P_{1,3}$ for the relevant two-fold coincidence events $CC_{4,2}$, $CC_{4,3}$, $CC_{1,2}$, $CC_{1,3}$.

- For Channels 1 and 2 we obtain:

$$P_{1,2} = |\beta|^2 R_1 T_1 \left(R_2 T_3 R_4 T_5 + T_2 R_3 T_4 R_5 + 2\sqrt{R_2 T_2 R_3 T_3 R_4 T_4 R_5 T_5} \cos \xi \right), \quad (45)$$

$$V_{1,2} = \frac{2\sqrt{R_2 T_2 R_3 T_3 R_4 T_4 R_5 T_5}}{R_2 T_3 R_4 T_5 + T_2 R_3 T_4 R_5}. \quad (46)$$

- For Channels 1 and 3 we obtain:

$$P_{1,3} = |\beta|^2 R_1 T_1 \left(R_2 T_3 R_4 R_5 + T_2 R_3 T_4 T_5 + 2\sqrt{R_2 T_2 R_3 T_3 R_4 T_4 R_5 T_5} \cos \xi \right), \quad (47)$$

$$V_{1,3} = \frac{2\sqrt{R_2 T_2 R_3 T_3 R_4 T_4 R_5 T_5}}{R_2 T_3 R_4 R_5 + T_2 R_3 T_4 T_5}. \quad (48)$$

- For Channels 4 and 2 we obtain:

$$P_{4,2} = |\beta|^2 R_1 T_1 \left(R_2 T_3 T_4 T_5 + T_2 R_3 R_4 R_5 + 2\sqrt{R_2 T_2 R_3 T_3 R_4 T_4 R_5 T_5} \cos \xi \right), \quad (49)$$

$$V_{4,2} = \frac{2\sqrt{R_2 T_2 R_3 T_3 R_4 T_4 R_5 T_5}}{R_2 T_3 T_4 T_5 + T_2 R_3 R_4 R_5}. \quad (50)$$

- For Channels 4 and 3 we obtain

$$P_{4,3} = |\beta|^2 R_1 T_1 \left(R_2 T_3 T_4 R_5 + T_2 R_3 R_4 T_5 + 2\sqrt{R_2 T_2 R_3 T_3 R_4 T_4 R_5 T_5} \cos \xi \right), \quad (51)$$

$$V_{4,3} = \frac{2\sqrt{R_2 T_2 R_3 T_3 R_4 T_4 R_5 T_5}}{R_2 T_3 T_4 R_5 + T_2 R_3 R_4 T_5}. \quad (52)$$

As an additional source of noise, we also take into account partially distinguishable photons with HOM visibility V_{HOM} . The result is that all four visibilities are scaled of the same factor $m = V_{HOM}$.

Let us now define the following four parameters:

$$x := \frac{T_2 R_3}{R_2 T_3}; \quad y := \frac{T_4}{R_4}; \quad z := \frac{T_5}{R_5}; \quad w := 2m\sqrt{xyz}. \quad (53)$$

In this way, we can rewrite the four visibilities as:

$$\begin{cases} V_{1,2} = \frac{w}{xy+z}, \\ V_{1,3} = \frac{w}{xyz+1}, \\ V_{4,2} = \frac{w}{x+yz}, \\ V_{4,3} = \frac{w}{y+xz}. \end{cases} \quad (54)$$

Through this parametrization, we are able to retrieve some relations between the visibilities, the reflectivity of the BSs and the photons indistinguishability parameters. Indeed, after some calculations, we retrieve:

$$\begin{cases} z = \frac{t_2+t_3-t_1^2-1 \pm \sqrt{(t_2+t_3-t_1^2-1)^2-4(t_2t_3-t_1)^2}}{2(t_2t_3-t_1)}, \\ x = \frac{t_2-t_3z}{t_1-z}, \\ y = \frac{t_3-zt_2}{t_1-z}, \\ w = \frac{V_{1,2}(1-z^2)}{t_1-z}, \end{cases} \quad \begin{cases} t_1 := \frac{V_{1,2}}{V_{1,3}}, \\ t_2 := \frac{V_{1,2}}{V_{4,2}}, \\ t_3 := \frac{V_{1,2}}{V_{4,3}}. \end{cases} \quad (55)$$

where the sign is chosen such that $z \geq 0$. We will use such relations to validate our experimental results, as described in the following subsection.

C. Entanglement swapping results analysis

We first report the measured visibilities in our apparatus:

$$\begin{cases} V_{A_1,C} = 0.942 \pm 0.002 \\ V_{A_1,B} = 0.862 \pm 0.002 \\ V_{A_2,C} = 0.879 \pm 0.002 \\ V_{A_2,B} = 0.903 \pm 0.002 \end{cases} \quad V_{\text{ave}} = 0.896 \pm 0.001. \quad (56)$$

obtained at the four output combinations of the entanglement swapping protocol. To validate the experiment, we compare these results with the model derived above. We first assume that the BS reflectivities have the ideal values:

$$R_2 = R_3 = R_4 = R_5 = 0.5, \quad (57)$$

while $V_{HOM} = 0.902$ is the Hong-Ou-Mandel visibility averaged over the two MZI interferometers. In this case, we find that the expected visibility for all possible two-fold events amounts to $V^{\text{theo}} = 0.902$. The difference between the theoretical prediction and the experimental one can be attributed to unbalanced splitting ratios of the various BSs and to different coupling and detection efficiencies in the apparatus. All these effects can be summarized by considering non-ideal reflectivities of the BSs.

If we follow the inverse approach, using the equations 55 and deriving the reflectivities of the BSs from the experimental visibilities we obtain:

$$x = 1.16 \pm 0.11; \quad R_4 = 0.44 \pm 0.04; \quad R_5 = 0.38 \pm 0.08; \quad V_{HOM} = 0.92 \pm 0.04. \quad (58)$$

These value are compatible with the parameters of the experimental apparatus.

V. CHARACTERIZATION OF THE SINGLE-PHOTON SOURCE

We characterize the single-photon purity of our source by measuring the second-order auto-correlation function in a Hanbury-Brown-Twiss interferometer at both Alice's and Bob's stations. Here, we show the normalized coincidences as a function of the delay in one of the two arms of the interferometer for both stations in Fig. 4a-b. The single-

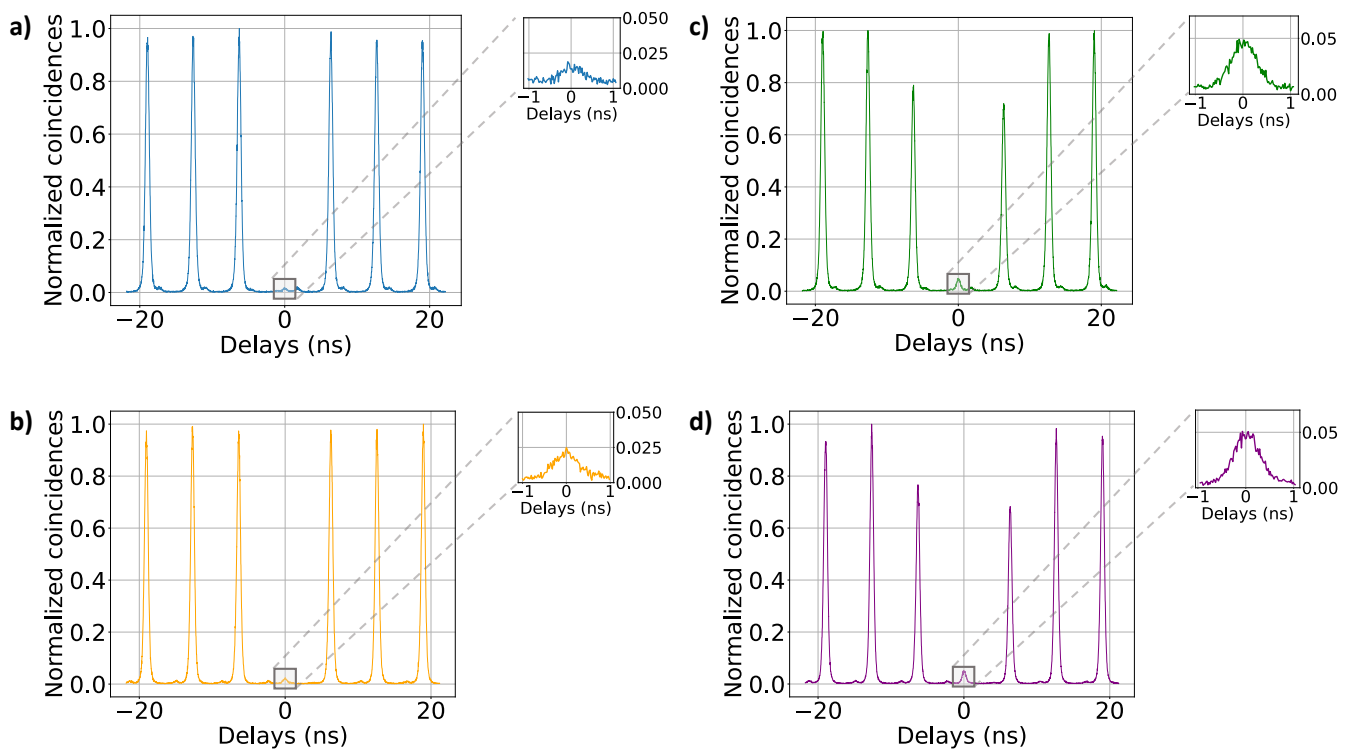


Figure 4. **Characteristics of our source.** a)-b) Plot of the normalized coincidences against time delay in a Hanbury-Brown-Twiss interferometer for the measurement of the second-order autocorrelation $g_2(0)$ of respectively Alice's and Bob's stations. c)-d) Plot of the normalized coincidences against time delay between in a Mach-Zehnder interferometer for the measurement of the HOM visibility V_{HOM} of respectively Alice's and Bob's stations.

photon indistinguishability is characterized by measuring the HOM visibility of two consecutive photons in a MZI interferometer as the one shown in Fig. 2b of the main text, for both Alice's and Bob's stations. Here, we show the normalized coincidences as a function of the delay in one of the two arms of the interferometer for both stations in Fig. 4c-d.

Finally, we report typical values of such quantities throughout the whole experiment:

$$\begin{aligned} g_2^{\text{Alice}}(0) &= 0.0146 \pm 0.0006 \\ g_2^{\text{Bob}}(0) &= 0.0192 \pm 0.0007 \\ V_{\text{HOM}}^{\text{Alice}} &= 0.9055 \pm 0.0015 \\ V_{\text{HOM}}^{\text{Bob}} &= 0.8987 \pm 0.0012 \end{aligned} \tag{59}$$